

# Unsupervised motion segmentation in one go: Smooth long-term model over a video

Etienne Meunier and Patrick Bouthemy

Inria, Centre Rennes - Bretagne Atlantique, France

October 3, 2023

## Abstract

Human beings have the ability to continuously analyze a video and immediately extract the main motion components. Motion segmentation methods often proceed frame by frame. We want to go beyond this classical paradigm, and perform the motion segmentation over a video sequence in one go. It will be a prominent added value for downstream computer vision tasks, and could provide a pretext criterion for unsupervised video representation learning. In this perspective, we propose a novel long-term spatio-temporal model operating in a totally unsupervised way. It takes as input the volume of consecutive optical flow (OF) fields, and delivers a volume of segments of coherent motion over the video. More specifically, we have designed a transformer-based network, where we leverage a mathematically well-founded framework, the Evidence Lower Bound (ELBO), to infer the loss function. The loss function combines a flow reconstruction term involving spatio-temporal parametric motion models combining, in a novel way, polynomial (quadratic) motion models for the  $(x, y)$ -spatial dimensions and B-splines for the time dimension of the video sequence, and a regularization term enforcing temporal consistency on the masks. We report experiments on four VOS benchmarks with convincing quantitative results. We also highlight through visual results the key contributions on temporal consistency brought by our method.

## 1 Introduction

When dealing with videos, motion segmentation is one of the key issues. Human beings have the ability to continuously analyze a video and immediately extract the main motion components. Computer vision methods usually proceed frame by frame. We want to go beyond this classical paradigm and segment the different motion entities in a video sequence in one go. We thus thoroughly investigate the temporal dimension of the motion segmentation problem. Since the optical flow (OF) yields all the information on the movement between two images of the video sequence, it is natural to base motion segmentation on optical flow. Motion segmentation is a computer vision task in its own, but it is also useful for diverse downstream tasks as independent moving object

detection, object tracking, or action recognition, to name a few. It is also leveraged in video object segmentation (VOS), while most often coupled with appearance.

The optical flow field at time  $t$  enables to get the segmentation at frame  $t$  of the video. However, taking a large time window, and even the whole video sequence, is beneficial, since motion entities are generally consistent throughout a video sequence (or at least within every video shot for long videos). Indeed, temporal coherence is inherent to motion. Therefore, it is essential that motion segmentation takes advantage of it, especially in a long-term perspective.

In this paper, we propose an original holistic method for multiple motion segmentation from optical flow over a video sequence. To the best of our knowledge, our optical flow segmentation (OFS) method is the first fully unsupervised network to involve long-term temporal consistency, and to segment multiple motions in a video sequence in one go. The main contributions of our work are as follows. Our network takes as input a volume of consecutive optical flows, and delivers consistent motion segmentation maps throughout the video sequence. It involves a transformer module allowing for long-term interactions. It is trained in a completely unsupervised manner, without any manual annotation or ground truth data of any kind. The loss function is inferred by leveraging the Evidence Lower Bound (ELBO) framework, and comprises a flow reconstruction term with original spatio-temporal parametric motion models and an additional term enforcing temporal consistency on the segmentation masks. We model with B-splines the long-term temporal evolution of the motion model parameters. Our method also involves a latent representation of the segment motion augmented with positional embedding.

The rest of the paper is organized as follows. Section 2 describes related work regarding motion segmentation. Section 3 presents our unsupervised network for multiple motion segmentation in one go, embedding long-term temporal consistency. In Section 4, we provide implementation details. Section 5 reports results on four VOS benchmarks with a comparison to state-of-the-art unsupervised motion segmentation methods. Finally, Section 6 contains concluding remarks.

## 2 Related work

Motion segmentation aims to break down each frame of a video sequence into components (or segments) of coherent motion. Usually, each motion segment is identified by a motion model, which can be hand-crafted such as affine or quadratic polynomial models or sometimes learned. Motion segmentation has been investigated for decades [19, 23, 38]. However, we will focus on recent methods in this section. Since accurate and efficient methods for estimating optical flow are now available, motion segmentation methods can leverage optical flow as a reliable input. The advent of deep learning methods in computer vision, and more recently the use of transformer-based networks with attention mechanisms [11], has also encompassed motion segmentation.

In [35], a transformer module, more specifically, the slot attention mechanism introduced in [18], is leveraged to perform motion segmentation from the optical flow. As a matter of fact, it addresses a binary segmentation problem, foreground moving object vs background. The loss function is composed of two terms, a flow reconstruction term

and an entropy term to make masks as binary as possible. Another approach is adopted in [34] that is able to cope with multiple motion segmentation. Nonlinear subspace filters are learned from stacked deep multi-layer perceptrons. Then, motion segmentation is inferred at inference by applying  $K$ -means to the output embeddings. In [21], the Expectation-Maximization (EM) framework is leveraged to define the loss function and the training procedure for an unsupervised frame-by-frame motion segmentation, where 12-parameter quadratic motion models are involved. The same authors also proposed an extension of that method in [22] to better handle the temporal dimension of the problem, by considering triplets of flows as input. In [36], the authors developed an adversarial method whose aim is to generate a mask hiding the input optical flow, where an inpainter network attempts to recover the flow within the mask. The rationale is that no correct reconstruction of the inside flow can be achieved from the outside flow, if the hidden area exhibits an independent motion and then constitutes a motion segment.

The temporal dimension of motion segmentation has been considered in various ways [30]. Regarding deep learning approaches, motion segmentation at time  $t$  is improved at training time in [35], by taking, as input, flows between  $t$  and several time instants before and after  $t$ . The authors of [8] consider several consecutive RGB frames as input of their self-supervised method. Optical flow is only computed at training time, and the loss function also comprises a temporal consistency term. However, the latter is not applied to two consecutive segmentation masks, but for pairings between the same frame  $t$  and another (more or less distant) one. In [9], spatio-temporal transformers were designed for video object segmentation involving temporal feature propagation.

VOS usually requires motion segmentation, often coupled with appearance [5, 10, 37]. It was addressed with supervised or semi-supervised methods as in [7, 9, 12], but also with unsupervised methods [36, 35, 21]. VOS is concerned with the segmentation of primary objects, i.e., object moving in the foreground of a scene and possibly tracked by the camera [39]. Thus, VOS generally involves binary ground truth segregating primary moving object against background. This is for instance the case for the DAVIS2016 benchmark [26]. Recent works have revisited the way of coupling appearance and motion for VOS. The AMD method [17] includes two pathways, the appearance one and the motion one. If it does not use optical flow as input and brings out the objectness concept, it nevertheless relies on a coarse motion representation. The RCF method [16] involves learnable motion models, and is structured in two stages, a motion-supervised object discovery stage, and then, a refinement stage with residual motion prediction and high-level appearance supervision. However, the method cannot distinguish objects undergoing different motions. In [6], the prediction of probable motion patterns is used at the training stage as a cue to learn objectness from videos. Divided attention is promoted in [14]. The resulting DivA method is based on the same principle as in [36] that motion segments are mutually uninformative. However, it is not limited to binary segmentation. It can segment a variable number of moving objects from optical flow, by leveraging a slot attention mechanism guided by the image content through a cross-modal conditional slot decoder.

Our fully unsupervised approach differs from these previous works in several respects. We rely only on optical flow and take a volume of OF fields as input, providing a volume of consistent segmentation maps. We introduce B-splines to define paramet-

ric motion models able to correctly handle motion evolution over time, and we express long-term temporal consistency. We infer the loss function from the Evidence Lower Bound (ELBO) framework. In [22], the authors also deal with temporal consistency. However, they only took a triplet of optical flow fields as input, they did not resort to transformers, and the temporal part of the motion model was just a linear (first-order polynomial) model in time. In addition, their temporal linkage of the consecutive motion segmentations over a video sequence was an *ad hoc* post-processing. In contrast, we define a fully integrated long-term model that is end-to-end trained in a unsupervised way. We will call our method LT-MS method, for long-term motion segmentation, and in contrast, we will refer to the method [22] as the ST-MS method, for short-term motion segmentation.

### 3 Long-term Motion Segmentation Method

We have designed a transformer-based network for multiple motion segmentation from optical flow. It is inspired from the MaskFormer architecture [4], but it only comprises one head corresponding to the mask prediction, as described in Fig.1. The network takes as input a volume, of flexible temporal length, comprising several consecutive optical flow fields. Temporal consistency is expressed in two main ways at the training stage. Firstly, we associate a space-time motion model with each segment to characterize its motion along with the evolution of the latter over time. Secondly, the loss function comprises an additional term enforcing consistent labeling of the motion segments over the volume.

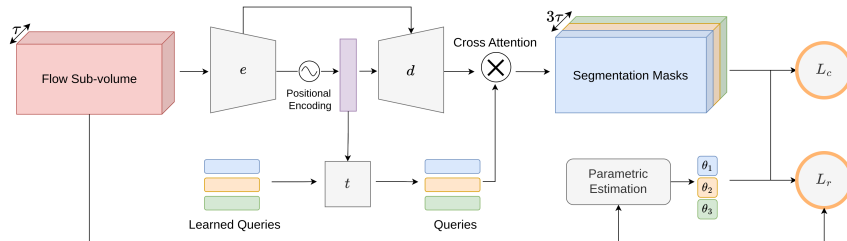


Figure 1: Overall architecture of our multiple motion segmentation method ensuring temporal consistency with the loss term  $\mathcal{L}_c$  and the B-spline space-time motion models  $\theta_k$  (for  $k = 1, \dots, K$ ). It takes as input a volume of  $T$  flow fields. It comprises a 3D U-net ( $e$  and  $d$  boxes) and a transformer decoder ( $t$  box). It also involves positional encoding. A cross-attention product yields the  $K$  segmentation masks corresponding to the input volume. For the sake of clarity, the block diagram is represented for three motion segments ( $K = 3$ ).  $\mathcal{L}_r$  is the flow-reconstruction loss term.

### 3.1 Spatio-temporal parametric motion model

The set of  $T$  consecutive flows will be designated as a space-time volume (or volume, to make it short). The volume could even be the whole video sequence. Our space-time motion model is estimated through B-spline functions [32]. We assign a spatio-temporal parametric motion model  $\tilde{f}_{\theta_k}$  to each motion segment  $k, k = 1, \dots, K$ .  $\theta_k$  specifies the motion model  $\tilde{f}$  for segment  $k$ . The motion model involves  $J$  parameters and each parameter  $\theta_{k_j}, j = 1, \dots, J$ , of the model results from a B-spline function of order  $n$  in the variable  $t$  over the space-time volume. In practice, we take  $n = 3$ . The number  $L$  of control points is given by  $L = 2 + \lfloor \frac{T-2}{\nu} \rfloor$ , where  $\nu$  allows us to set the temporal frequency of control points. We put a control point at both ends of the volume (at  $t = 1$  and  $t = T$ ), and the other control points are equidistantly placed between the two. Most often, the control points are not located at time points of the video sequence.

The space-time spline-based motion model is illustrated in Fig.2. Just for this illustration, the motion models are computed within the two segments, foreground moving object and background, provided by the ground truth. The estimated motion model for the foreground moving object is able to capture the periodic nature of the swing motion as demonstrated by the plots of the computed motion model parameters. Also, the motion model computed in the background segment perfectly fits the camera motion. Articulated motion (woman’s legs) would require multiple-motion segmentation.

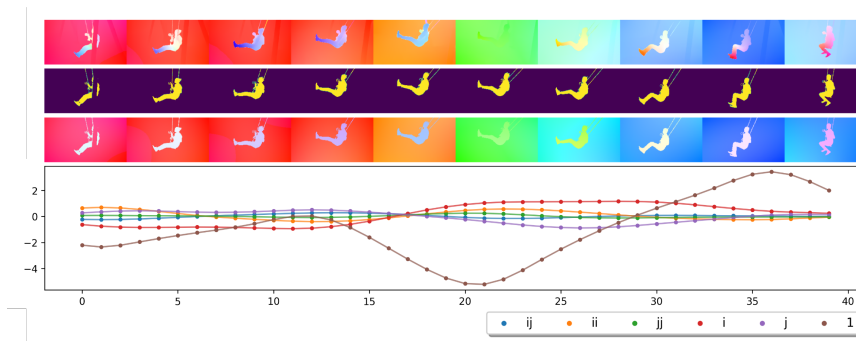


Figure 2: Illustration of the spatiotemporal spline-based motion model. Top row: input flows displayed with the HSV code for the *swing* video of DAVIS2016 dataset, binary segmentation ground truth, flows generated by the estimated spline-based motion models for the two segments. Bottom row: plot of the temporal evolution of the six estimated model parameters corresponding to the flow  $u$ -coordinate for the foreground moving object.

Any parametric motion model could be considered. We use the 12-parameter quadratic motion model to be able to account for continuously varying depth surface of the objects in the scene, especially for the whole background, and for complex object or camera motions. In contrast, the affine and the 8-parameter quadratic motion models assume a planar object surface. Indeed, the latter exactly corresponds to the projection in the image of the 3D rigid motion of a planar surface. It is equivalent for velocity fields to the homography transform. However, in presence of severe depth

effects (strong depth discontinuities) and camera motion, the static scene cannot be represented by a single motion model due to motion parallax produced by static objects located in the foreground. Regarding first the spatial dimension of the motion model, the 2D flow vector yielded by the full quadratic motion model at point  $(x, y)$  writes:

$$\tilde{f}_\theta(x, y) = (\theta_1 + \theta_2 x + \theta_3 y + \theta_7 x^2 + \theta_8 xy + \theta_9 y^2, \theta_4 + \theta_5 x + \theta_6 y + \theta_{10} x^2 + \theta_{11} xy + \theta_{12} y^2)^T. \quad (1)$$

To correctly handle complex temporal evolution, we resort to the spline approximation as aforementioned. By denoting now  $S_n(\theta_k)$  the subscript of  $\tilde{f}$ , we emphasize that the motion model parameters for each segment  $k$  are estimated through the B-spline functions. More specifically, we have:

$$\tilde{f}_{S_n(\theta_k)}(i, t) = \sum_{l=1}^L \tilde{f}_{\theta_{k,l}}(i, t) B_{n,l}(t), \quad (2)$$

where  $B_{n,l}$  is the  $l^{\text{th}}$  B-spline and  $\theta_{k,l}$  corresponds to the  $l^{\text{th}}$  control point of the spline function.

### 3.2 Loss function

We consider a volume of optical flow fields  $f \in \mathbb{R}^{2 \times T \times W \times H}$ , the spatial grid  $\Omega \in \mathbb{R}^{W \times H}$  and  $T$  temporal steps. We denote  $f(i, t) \in \mathbb{R}^2$  the flow associated to site  $i \in \Omega$  at time  $t$ . We assume that we can decompose the flow as a set of  $K$  segments, each one exhibiting a coherent motion. Flow vectors within a given segment  $k$  are represented by a smooth parametric motion model parametrized by  $\vartheta_k$ . Variable  $z_{i,t}$  conveys the motion segmentation,  $z_{i,t}^k = 1$  if site  $(i, t)$  belongs to segment  $k$ .  $z$  and  $\vartheta = \{\vartheta_k, k = 1 \dots K\}$  are latent variables, and  $f$  is the observed data. Following [13], we introduce an approximate distribution over segmentation and motion model parameters:

$$q(z, \vartheta | f) = q(z | f) q(\vartheta) = \left( \prod_{t=1}^T \prod_{i \in \Omega} \prod_{k=1}^K q(z_{i,t}^k | f) \right) \left( \prod_k q(\vartheta_k) \right), \quad (3)$$

where  $q(\vartheta_k) \triangleq \delta(\vartheta_k)$  with  $\delta$  the dirac distribution and  $q(z_{i,t}^k | f) = g_\phi(f)_{i,t}^k$ .  $g_\phi$  is our network model taking as input the optical flow volume and returning a probabilistic segmentation volume.

We can also write the data-likelihood over a dataset  $\mathcal{D}$  of optical flow volumes  $f$  as:

$$\begin{aligned} \log(\mathcal{D}) &= \sum_{f \in \mathcal{D}} \log p(f) = \sum_{f \in \mathcal{D}} (\mathbb{E}_{q(z, \vartheta | f)} [\log \frac{p(f, z, \vartheta)}{q(z, \vartheta | f)}] + KL(q(z, \vartheta | f) || p(z, \vartheta | f))) \\ &\geq \sum_{f \in \mathcal{D}} (\mathbb{E}_{q(z, \vartheta | f)} [\log p(f | z, \vartheta)] - KL(q(z, \vartheta | f) || p(z, \vartheta))), \end{aligned} \quad (4)$$

where we obtain the Evidence Lower Bound (ELBO). Following the assumption stated above, we can write our likelihood as:

$$p(f|z, \vartheta) = \prod_{t=1}^T \prod_{k=1}^K p(f(t)|\vartheta_k, z) \quad (5)$$

$$\propto \prod_{t=1}^T \prod_{k=1}^K \prod_{i \in \Omega} \exp(-\|f(i, t) - \tilde{f}_{S_n(\vartheta_k)}(i, t)\|_1 / \xi_{f,t})^{z_{i,t}^k}, \quad (6)$$

where  $\tilde{f}_{S_n(\vartheta_k)}(i, t)$  is the flow vector given by the parametric motion model of parameters  $\vartheta_k$  at point  $(i, t)$  as defined in Section 3.1 through the spline approximation and  $\xi_{f,t} = \sum_i \|f(i, t)\|_1$  is a normalizing factor. From this likelihood, we can write the left term of the ELBO as:

$$\mathcal{L}_r = -\mathbb{E}_{q(z, \vartheta|f)}[\log p(f|z, \vartheta)] \quad (7)$$

$$\begin{aligned} &= -\sum_{t=1}^T \sum_k \mathbb{E}_q[\log p(f(t)|\vartheta_k, z)] \\ &= \sum_{t=1}^T \sum_{i \in \Omega} \sum_k g_\phi(f)_{i,t}^k \|f(i, t) - \tilde{f}_{S_n(\theta_k)}(i, t)\|_1 / \xi_{f,t} \end{aligned} \quad (8)$$

The term  $KL(q(z, \vartheta|f)||p(z, \vartheta))$  allows us to define a prior over the segmentation. We want to enforce the property that the segmentation labels are temporally consistent, i.e., similar between neighbouring frames. We approximate this term using the temporal consistency loss defined in [22], as it showed good experimental results and was efficient to compute at training time:

$$\mathcal{L}_c = \frac{1}{2K|\mathcal{I}|} \sum_{i \in \Omega} \sum_{t=2}^T \mathbb{1}[\|f_{i,t} - f_{i,t-1}\|_1 < \lambda] \sum_{k=1}^K |g_\phi(f)_{i,t}^k - g_\phi(f)_{i,t-1}^k|, \quad (9)$$

The threshold  $\lambda$  allows us to discard occlusion areas. The loss function is thus defined by:

$$\sum_{f \in \mathcal{D}} \mathcal{L}(f, \phi, \theta) = \sum_{f \in \mathcal{D}} \mathcal{L}_r(f, \phi, \theta) + \beta \mathcal{L}_c(f, \phi). \quad (10)$$

We set  $\beta = 1$ . The training procedure alternatively updates  $\theta$  and  $\phi$  with  $\alpha$  as learning rate:

$$\text{for } f \in D : \theta^* = \arg \min_{\theta} L(f, \phi, \theta)(f) ; \phi_{t+1} = \phi_t - \alpha \nabla_{\phi} L(f, \phi, \theta^*) \quad (11)$$

### 3.3 Network architecture

The overall architecture of our unsupervised multiple motion segmentation framework is illustrated in Fig.1. It includes two main modules. The first one, taking the flow volume as input, is a 3D U-net [29]. The latent code augmented with embedding positions

is directed to the transformer decoder. Then, by cross-attention, the output formed by the volume of segmentation masks is produced. The training of the overall architecture is based on the minimization of the loss function defined below, while the motion model parameters of the segments are given by the B-spline estimation. Temporal consistency is provided by the loss function and the space-time motion models.

## 4 Implementation

### 4.1 Implementation details

Following [6, 16, 21, 22, 35], we adopt the RAFT method [31] to compute the optical flow fields. More specifically, we use the RAFT version trained on the MPI Sintel dataset [2]. We downsample the computed flow fields to feed the network with  $128 \times 224$  vector fields. The output segmentation maps are upsampled to the initial frame size for evaluation. Thus, we can perform efficient training and inference stages. We typically take flow volumes of temporal length  $T = 9$  at training time. However, at test time, we can process flow volumes of larger temporal length, and even the flow volume of the whole sequence. To compute of the spatio-temporal parametric motion models,  $x$  and  $y$  coordinates are normalized within  $[-1, 1]$ , and a similar normalization is applied to the  $t$  coordinate. The full 12-parameter quadratic motion model is chosen in all the experiments, and we take  $\nu = 3$  for the frequency factor in the B-spline approximation. We select for each site  $i$  the segment  $\hat{k}$  with the highest prediction. In eq.(9), we set  $\lambda$  as the 99<sup>th</sup> quantile of the flow differences over the flow volume.

Our LT-MS method is very efficient at test time. The computational time amounts on average to 210 *fps* on a GPU P100, that is, twice as fast as the ST-MS method [22]. It is certainly due to the long flow sequence given as input to the network, which allows for parallelisation of some heavy computations. In addition, our LT-MS architecture remains lightweight, since it combines only three Unet layers and a transformer decoder on the downsampled feature space. Let us also stress that our LT-MS method does not involve any post-processing at all.

### 4.2 Data augmentation and network training

We applied two types of data augmentation dedicated to optical flow. First, we add a global flow to the input flow similarly as in the EM [21] and ST-MS [22] methods. However, in our case, the global flow is given by a full spline-based spatio-temporal motion model whose parameters are chosen at random. The same global flow is added to the flow fields of a given input volume. It allows us to mimic diverse camera motions, enforcing that the motion segments are independent of it. In addition, we corrupt a few flows out of the nine input ones. Thus, we simulate poorly estimated flow fields at some time instants, and the temporal consistency should overcome it.

Our motion segmentation method is fully unsupervised. We never use any manual annotation. We train our model only with the FlyingThings3D (FT3D) dataset [20], whatever the dataset considered at test time. This ensures that our LT-MS network generalizes well to unseen datasets. Regarding hyperparameter setting, we select the

stopping epoch from the loss function evaluated on the DAVIS2016 training set. Additional information on the optimization stage is given in the Appendix.

## 5 Experimental Results

We have carried out comparative experiments on four datasets: DAVIS2016<sup>1</sup> [26], SegTrackV2<sup>2</sup> [15], FBMS59 [24], and DAVIS2017-motion [33]. More information on the datasets is provided in the Appendix.

### 5.1 Ablation study

We have conducted an ablation study to assess three main components of our method LT-MS with four masks ( $K = 4$ ), in particular related to the temporal dimension of the problem. We have changed one component at a time as specified hereafter. We use the polynomial space-time quadratic motion model of ST-MS [22] instead of the space-time motion model based on B-splines over the input sequence. We omit the consistency term  $\mathcal{L}_c$  in the loss function. We just take the convnet without the transformer decoder. All the ablation experiments were run on the three datasets, DAVIS2016, FBMS59, SegTrackV2. Results are collected in Table 1. In addition, we performed them for two input sequence configurations, respectively input sequences of ten flows, and input sequence of 120 flows (in practice, the whole video for the DAVIS2016 dataset). We can observe that the three ablations have almost the same impact on the performance. The three corresponding model components, i.e., the spline-based motion model, the temporal-consistency loss term, and the transformer decoder are thus all beneficial in similar proportions. They are able to handle the temporal dimension of the problem and the temporal motion evolution along the sequence in a compelling way. Admittedly, the contributions of these three components are more significant for the FBMS59 and the SegTrackV2 datasets. However, the dynamic content of the majority of the DAVIS2016 videos, and then, the overall performance score, cannot allow us to fully appreciate the contributions of these three model components. Yet, they can be acknowledged by visualizing results obtained on some videos of DAVIS2016, as shown in the Appendix.

### 5.2 Quantitative and comparative evaluation

We report in Table 2 the results obtained by two versions of our LT-MS method on the three datasets DAVIS2016, SegTrackV2, and FBMS59. LT-MS-K2 performs segmentation with only two masks ( $K = 2$ ) while LT-MS-K4 involves four masks ( $K = 4$ ). Table 2 collects results obtained by our LT-MS method and other existing unsupervised methods, when available. We follow the categorization proposed in [21] regarding input and training. However, we have added a category w.r.t. the network input for four recent methods, [6, 8, 16, 17], that only use RGB images as input at test time, the optical flow being only involved in the loss function. Evaluation is performed on the

<sup>1</sup><https://davischallenge.org/index.html>

<sup>2</sup><https://paperswithcode.com/dataset/segtrack-v2-1>

Table 1: Ablation study for three main components of our method LT-MS ( $K = 4$ ) on DAVIS2016, FBMS59 and SegTrackV2. Only one model component is modified at a time. The performance scores are given by the Jaccard index  $\mathcal{J}$ . We report ablation results with two input-flow sequence length (or cut size), respectively, by dividing the video into pieces of ten successive frames or by considering 120 successive frames (in practice, the whole video for DAVIS2016).

Ablation / Dataset	DAVIS2016		FBMS59		SegTrackv2	
	10	120	10	120	10	120
Full Model LT-MS-K4	74.8	72.4	61.0	58.2	61.3	60.4
Unet3D only	73.0	71.3	56.6	55.5	58.2	57.3
No consistency term $\mathcal{L}_c$	73.5	71.0	57.5	55.5	58.0	57.5
Polynomial space-time quadratic model	73.4	69.8	57.4	54.5	57.8	56.6

binary ground truth (foreground moving object vs background) for the three datasets. In the Appendix, we explain how we select the segments for the binary evaluation from the multiple motion segments delivered by our LT-MS method. We still put the OCLR method [33] in the category of unsupervised methods, whereas the authors of the DivA method [14] did not. Indeed, OCLR is not fully unsupervised, since it relies on human-annotated sprites to include realistic shapes in the computer-generated data used at training time. We consider the OCLR version taking only optical flow as input. The post-processing added to the CIS method [36], based on Conditional Random Fields (CRF), is an heavy one, which leads most authors to retain only the version without post-processing for a fair comparison.

As shown in Table 2, our LT-MS method provides very convincing results, both for LT-MS-K2 and LT-MS-K4, in the category of unsupervised methods based on optical flow only. OCLR and DivA demonstrate better performance on the SegTrackV2 dataset. However, as aforementioned, OCLR is not a fully unsupervised method, while DivA leverages RGB images in its conditional decoder. In addition, DivA, along with MoSeg and CIS methods, takes multi-step flows as input between  $t$  and in turn  $t + 1$ ,  $t + 2$ ,  $t - 1$ ,  $t - 2$ , and averages the four corresponding predictions to get the final result. SegTrackV2 includes sequences acquired with a poorly controlled handheld camera, which leads to unstable sequences where the contribution of our method is therefore less likely to be emphasized.

Overall, temporal consistency is properly handled over long temporal periods by our LT-MS method. Beyond segmentation performance, we want to stress that our method is the only one providing *by design* a coherent segmentation over the sequence, which is a significant added value. Thus, we can claim that we have not only segmented the moving objects throughout the sequence, but also achieved some kind of tracking.

### 5.3 Multi-segment evaluation

We have also performed the evaluation of multiple motion segmentation for a multi-segment setting. Since multiple-motion segmentation is harder than the binary motion segmentation (moving foreground vs background), accuracy scores are expected to de-

Table 2: Results obtained with two versions of our LT-MS method on DAVIS2016, SegTrackV2, FBMS59. LT-MS-K2 performs segmentation with two masks ( $K = 2$ ), and LT-MS-K4 involves four masks ( $K = 4$ ). We include comparison with unsupervised methods (scores from cited articles). All scores corresponds to evaluation on the binary ground-truth. For LT-MS-K4 and LT-MS-K2, we report results obtained with a cut size of 10. Results with a cut size of 120 are given for LT-MS-K4 in Table 1 with very close performance (additional results on this point in the Appendix). The Jaccard index  $\mathcal{J}$  is the intersection over union between the extracted segments and the ground truth, while  $\mathcal{F}$  focuses on segment boundary accuracy. Performance is assessed by the average score over all samples, for all datasets but DAVIS2016. For the latter, the overall score is given by the average of sequence scores. \*Actually, putting OCLR as an unsupervised method can be questionable (see main text). †DivA somehow uses RGB input since its conditional decoder leverages input images.

Method	Training	Input	DAVIS2016		SegTrack V2	FBMS59	
			$\mathcal{J} \uparrow$	$\mathcal{F} \uparrow$	$\mathcal{J} \uparrow$	$\mathcal{J} \uparrow$	
<b>Ours LT-MS-K4</b>	Unsupervised	Flow	74.8	72.2	61.3	61.0	
<b>Ours LT-MS-K2</b>			70.3	68.5	58.6	55.3	
ST-MS (4 masks) [22]			73.2	70.3	55.0	59.4	
EM [21]			69.3	70.7	55.5	57.8	
MoSeg [35]			68.3	66.1	58.6	53.1	
FTS [25]			55.8	-	47.8	47.7	
TIS <sub>0</sub> [10]			56.2	45.6	-	-	
OCLR* [33] (flow only)			72.1	-	67.6	65.4	
GWM [6]			RGB (Flow in loss)	79.5	-	78.3	77.4
RCF [16]				80.9	-	76.7	69.9
AMD [17]		57.8		-	57.0	47.5	
MOD [8]		73.9		-	62.2	61.3	
DivA(4)† [14]		RGB & Flow	72.4	-	64.6	-	
TIS <sub>s</sub> [10]			62.6	59.6	-	-	
CIS - No Post [36]			59.2	-	45.6	36.8	
CIS - With Post [36]			71.5	-	62.0	63.6	

crease for all methods. In Table 3, we report comparative results on the DAVIS2017-motion dataset and on FBMS59. As for the other methods, we performed segmentation with three masks. To this end, we finetuned the LT-MS-K4 network on the DAVIS2016 training set with now three masks ( $K = 3$ ). The resulting performance on DAVIS2017-motion is slightly better than ST-MS [22], and far better than MoSeg. There is still the same remark about OCLR status as an unsupervised method. Regarding FBMS59, we report multimask segmentation results with two different metrics. Our LT-MS method outperforms by a large margin DivA [14] that attempted this multi-segment evaluation on FBMS59.

Table 3: Multi-segment evaluation. Regarding DAVIS2017-motion,  $\mathcal{J}\&\mathcal{F}$  is the mean of the two. Evaluation is performed on the video as a whole according to the official DAVIS2017 scheme. Reported scores are the average of the individual video scores. \*See caption of Table 2. For FBMS59, the two evaluation metrics are bootstrap IoU (bIoU) [14] where each ground-truth mask is mapped to the most likely predicted segment (performed at the frame level), and linear assignment that is a bilinear mapping between the ground-truth and the predicted segments at the sequence level (similar to the official DAVIS2017 evaluation).

Dataset	DAVIS2017-motion			FBMS59	
	$\mathcal{J}\&\mathcal{F} \uparrow$	$\mathcal{J} \uparrow$	$\mathcal{F} \uparrow$	bIoU	Linear Assignment
<b>Ours LT-MS-K3</b>	42.2	39.3	45.0	58.4	47.2
ST-MS [22]	42.0	38.8	45.2	-	-
MoSeg [35]	35.8	38.4	33.2	-	-
OCLR* [33]	55.1	54.5	55.7	-	-
DivA [14]	-	-	-	42.0	-

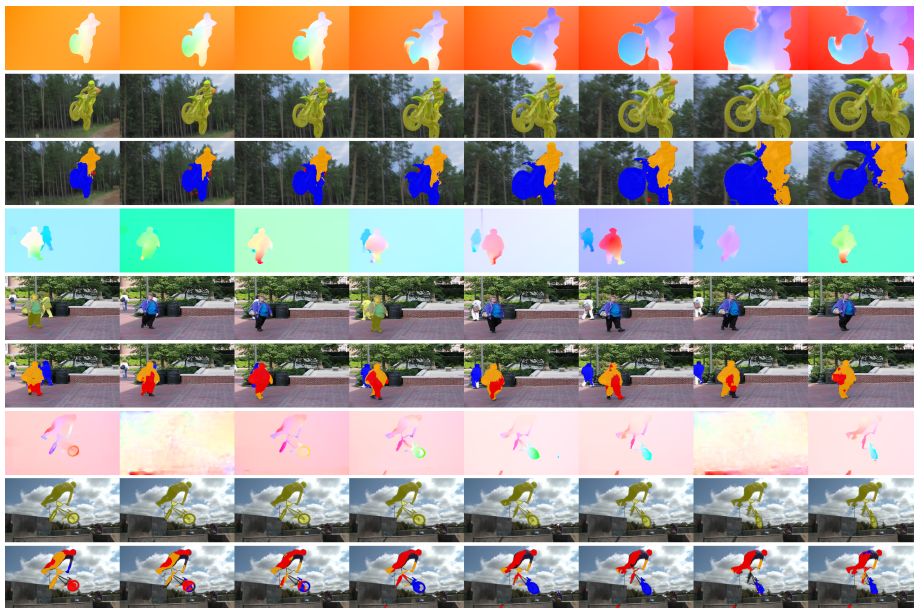


Figure 3: Results obtained with our LT-MS-K4 method ( $K = 4$ ). Three groups of results are displayed, *motocross-jump* from DAVIS2016, *people02* from FBMS59 and *bxm* from SegTrackV2. For each group, the first row samples successive flow fields (HSV color code) corresponding to the processed video. The second row contains the corresponding images of the video, where the ground-truth of the moving object is overlaid in yellow (when available at that frame). The third row shows the motion segments provided by our LT-MS-K4 method with one colour per segment. For all the results, we adopt the same color set for the three masks corresponding to the moving objects (blue, red and orange), and we let the background image for the background mask.

## 5.4 Qualitative visual evaluation

Fig.3 contains several visual results to demonstrate how our LT-MS method behaves on different situations. We display three result samples obtained on different videos of the benchmarks. Additional results are provided in the Appendix. We can observe that the motion segments are globally accurate. Since our method involves several masks, we can properly handle articulated motions (*people2*, *bmx*), deal with the presence of several moving objects in the scene (*people2*), separate the rider from the bike or motorbike (*bmx*, *motocross-jump*), or accomodate motion parallax. Since our method enforces temporal consistency, it can also deal with errors in optical flow estimation or with objects that momentarily stop moving (*bmx*). We must keep in mind that our actual target is the optical-flow segmentation (OFS) task, even if we evaluate our method on VOS benchmarks. When VOS benchmarks deal with the segmentation of one primary object moving in the foreground, it may occur discrepancies with OFS, which negatively impacts the evaluation scores. The segmentation of additional parts, which appears wrong w.r.t. VOS ground truth, on the contrary makes sense from the OFS standpoint.

## 6 Conclusion

We have designed an original transformer-based unsupervised method for segmenting multiple motions over a video in one go. Our LT-MS method leverages the ELBO framework for the loss function, and fully acknowledges the temporal dimension of the motion segmentation problem. Indeed, to the best of our knowledge, our method is the first unsupervised network-based OFS method explicitly leading to a stable and consistent OF segmentation throughout long video sequences. It introduces at training time, on one hand, B-splines spatio-temporal parametric motion models over space-time volumes, and on the other hand, a loss term expressing temporal consistency over successive masks while taking care of occlusions. Our transformer-based network can be applied at test time to input volumes of any time length. It can accomodate different choices on the number  $K$  of masks with a simple finetuning step. Experimental results on several datasets demonstrate the efficiency and the accuracy of our LT-MS method by providing competitive results on several datasets. In addition, it is very fast at test time. In future work, we will investigate the slot attention mechanism to modify the number of masks at test time without retraining the model.

## 7 Appendix

### 7.1 Datasets

DAVIS2016 comprises 50 videos (for a total of 3455 frames), depicting diverse moving objects. It is split in a training set of 30 videos and a validation set of 20 videos. Only the primary moving object is annotated in the ground truth. The criteria for evaluation on this dataset are the Jaccard score  $\mathcal{J}$  (intersection-over-union), and the contour accuracy score  $\mathcal{F}$ , the higher, the better for both. FBMS59 includes 59 videos (720 annotated frames), and SegTrackV2 14 videos (1066 annotated frames). Both mostly

involve one foreground moving object, but sometimes a couple of moving objects. For FBMS59, we use the 30 sequences of the validation set. Although annotations may comprise multiple objects, the VOS community exploits FBMS59 and SegTrackV2 similarly as DAVIS2016, considering a binary ground-truth, by grouping moving objects in the foreground. We follow this practice. However, we also provide a multi-mask evaluation for FBMS59.

DAVIS2017 is an extension of DAVIS2016, containing 90 videos. It includes additional videos with multiple moving objects, and it provides multiple-segment annotations for the ground truth. It is split into 60 videos for training and 30 for evaluation. DAVIS2017-motion is a curated version of the DAVIS2017 dataset proposed in [33] for a fair evaluation of methods based on optical flow only. Connected objects exhibiting the same motion are merged in the ground truth for evaluation. We proceed to the evaluation with the official algorithm that involves a Hungarian matching process.

## 7.2 Addition to the ablation study

Fig.4 plots the performance scores for the three ablations when the length of the input flow sequence varies from 10 to 120. Overall, they exhibit comparable behaviour at a certain distance from the full model.

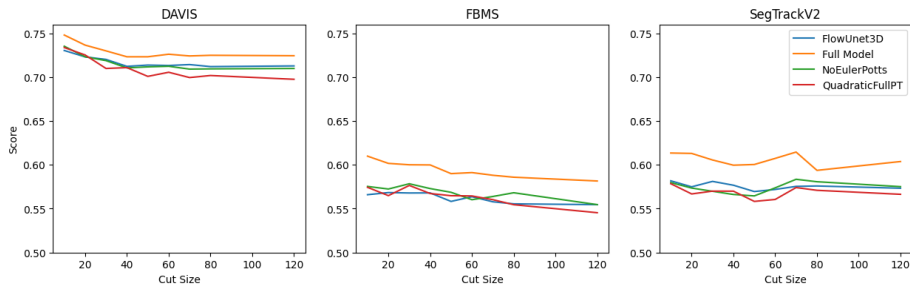


Figure 4: Influence of the length of the input flow sequence (also referred to as cut size on the horizontal axis of the plot) on the three modified versions of our LT-MS-K4 method with comparison with the full model. Left plot: for the DAVIS2016 dataset. Middle plot: for the FBMS59 dataset. Right plot: for the SegTrackV2 dataset. Overall, they exhibit comparable behaviour at a certain distance from the full model.

Visual results reported in Fig.5 clearly demonstrate that the addition of the temporal consistency loss term  $\mathcal{L}_c$  allows us to get far more consistent segments over time, whether for the background, or the moving objects. For instance, in the fourth example, the foreground moving car is perfectly segmented throughout the sequence along with its wheels, and (small) moving cars in the background. Fig.7 highlights the contribution of the spline-based motion model on the *dog* video, and its obvious ability to handle motions that do not vary uniformly, as the erratic movement of the dog.

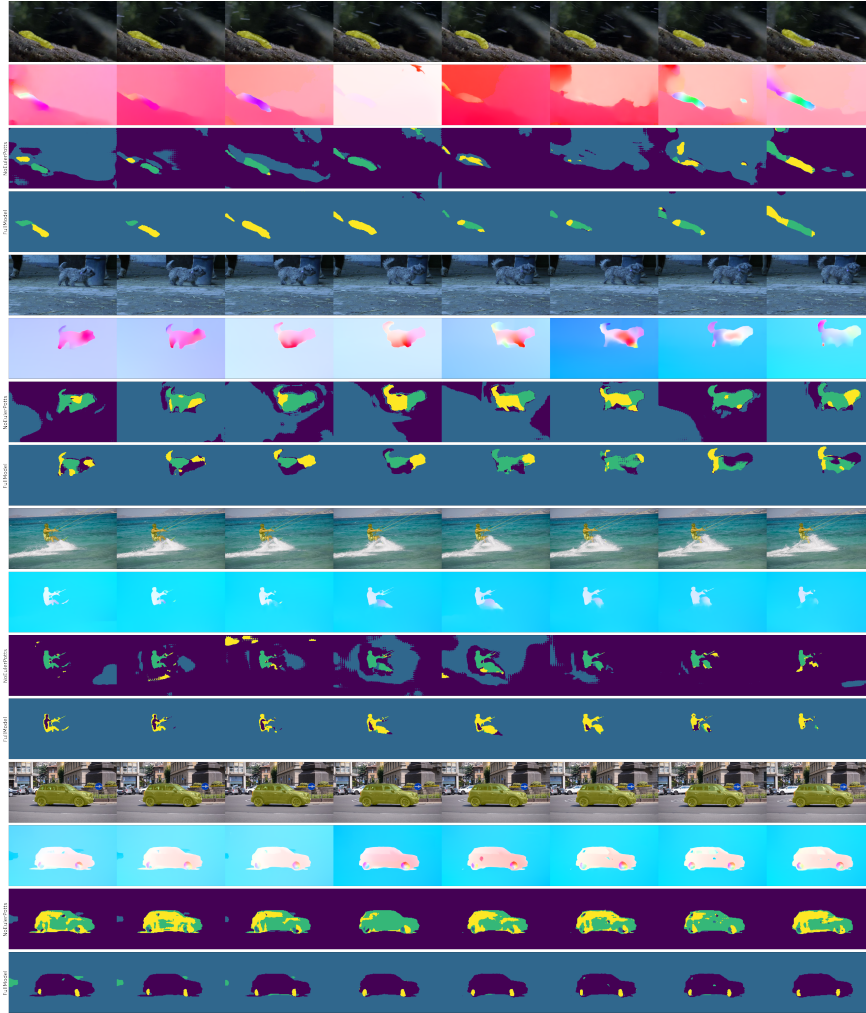


Figure 5: Four groups of qualitative results regarding the ablation of the temporal-consistency loss term. They respectively correspond to the *worm* video of SegTrackV2, the *dogs01* video of FBMS59, and the *kite-surf* and *car-roundabout* videos of DAVIS2016. For each group, the first row contains sample images with the segmentation ground-truth, when available at that frame, overlaid in yellow, the second row displays the input flows, the third and fourth rows show the predicted motion segmentations, respectively without and with the temporal consistency loss term. Clearly, this model component allows us to get far more consistent segments over time.

### 7.3 Optimization implementation

We use Adam optimizer with the following strategy on the learning rate  $\alpha$  to train the network (3D Unet and transformer), inspired from the warmup-decay strategy in [33]. We linearly increase it from 0 to  $1e - 4$  for 20 epochs, then, we divide it by two every 40 epochs. The estimation of the motion model parameters through the B-spline approximation at training time is achieved with the Pytorch implementation of L-BGFS [40].

### 7.4 Segment selection for evaluation

VOS and OFS are close but not identical tasks. However, we use VOS benchmarks, since no OFS benchmarks are available. Let us recall that the VOS one is attached to the notion of a primary object of interest moving in the foreground (sometimes, a couple of objects). As a consequence, we have to select the right segments to cope with the binary ground truth of the VOS benchmarks, as usually done for the DAVIS2016, SegTrackV2 and FBMS59 datasets.

Since we deal with multiple-motion segmentation, i.e.,  $K$  segments, we have to group them into two clusters corresponding to the foreground moving object on one side and the background on the other side. We proceed as in the ST-MS method [22]. However, in our case, we can directly evaluate our LT-MS method in one shot over the predicted segmentation sequence, since there is no temporal linking postprocessing for LT-MS. For evaluations with  $K = 2$ , we do not need to group the masks, so we just set one of the masks as foreground using Hungarian matching over the sequence (alternatively, we could just pick the smallest of the two masks). Regarding the evaluation on the DAVIS2017-motion dataset whose ground truth is not binary, we use the official evaluation script (which perform hungarian matching over the sequence) to associate each predicted segment  $k$  with the ground-truth annotations, knowing that we have to consider  $K = 3$  masks for this experimentation.

### 7.5 Multi-mask evaluation in FBMS59

We implement the "Bootstrap IoU" score to evaluate multi-mask segmentation in FBMS59, as described in [14]<sup>3</sup> The core idea is to match each ground-truth segment to the most likely segment (i.e., with the one of highest IoU). Let us note that this evaluation includes the background segment, since background is not identified in the FBMS59 multi-mask annotation. The algorithm we used for evaluation is detailed in Fig. 6.

For the linear assignment score, we find the best bipartite sequence-level match between the ground truth and the predictions. Similar to the bIoU evaluation, we compute the score with all the labels of the ground truth. This evaluation is more demanding, because it forces a one-to-one match between the prediction and the masks at the sequence level.

---

<sup>3</sup>We use the multi-label ground truth provided by Dong Lao, first author of [14].

```

1 sequences_iou = []
2 for sequence in dataset :
3     objects_iou = []
4     for frame in sequence :
5         for x in gt_annotations_including_background :
6             maxiou = 0
7             for y in predicted_segments :
8                 maxiou = max(maxiou, iou(x, y))
9                 objects_iou.append(maxiou)
10            sequence_iou.append(mean(objects_iou))
11 dataset_iou = mean(sequences_iou)

```

Figure 6: Algorithm Evaluation bIoU.

## 7.6 Influence of the cut size at inference

We have also tested how our LT-MS-K4 method behaves when varying the length of the input flow sequence. Results are plotted in Fig.8 for three datasets, DAVIS2016, FBMS59 and SegTrackV2. As expected, the best performance is obtained for the smallest length (equal to 10) of the input flow sequence. However, performance decreases slowly when the length increases, and remains stable for larger ones. It demonstrates the intrinsic ability of the LT-MS method to achieve accurate and consistent motion segmentation over long periods of the video, which is a unique property. We also did it for LT-MS-K2 as reported in Table 4. We even get slightly better results for DAVIS2016 and SegTrackV2 when the video sequence is processed in one go, i.e., with an infinite cutsize.

Table 4: Results obtained on the three datasets DAVIS2016, FBMS59 and SegTrackV2 with LT-MS-K2 for respectively a cut size of 10 and no cut (the video sequence is processed in one go).

Dataset	DAVIS2016		FBMS59		SegTrackV2	
Cut Size	10	$\infty$	10	$\infty$	10	$\infty$
LT-MS-K2	70.3	70.7	55.3	48.7	58.6	59.3

## 7.7 Additional visual evaluation

Additional visual results of our LT-MS method are provided in Fig.9. We can observe that the motion segments are globally accurate. Let us recall that the ground-truth is not necessarily available for all the video frames depending on the datasets. Since our method involves several masks, we can properly handle articulated motions (*monkey*), deal with the presence of several moving objects in the scene (*hummingbird*), or accommodate motion parallax (*libby*).

In Fig.10, we collect additional visual results on three videos of the SegTrackV2 dataset, from top to bottom, the *birdfall*, *bird-of-paradise*, and *bmX* videos. Results demonstrate the ability of our long-term segmentation method to recover, to some extent, correct segmentation even from flow fields wrongly computed at some time instants.

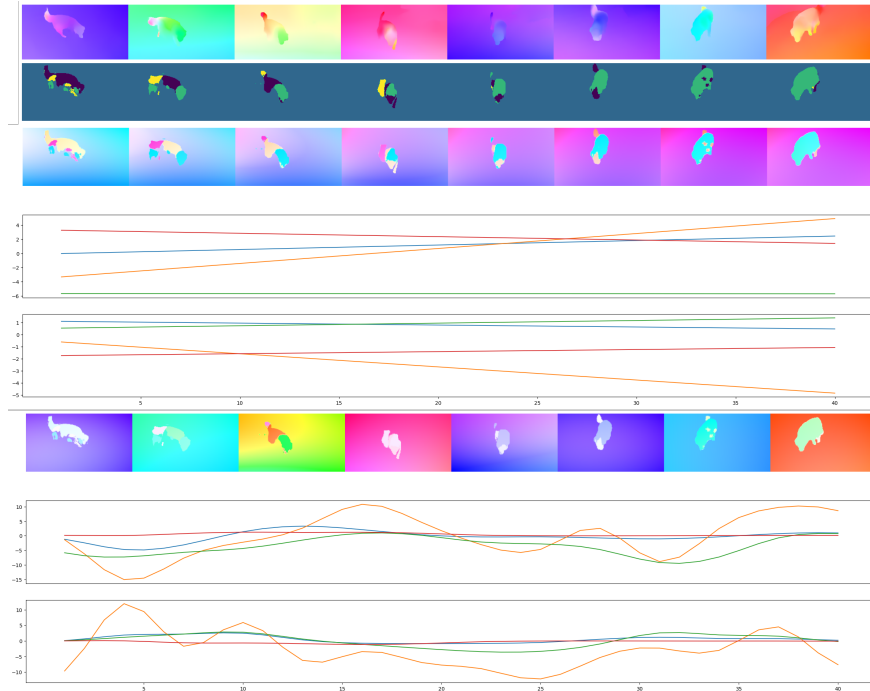


Figure 7: Visual assessment of the contribution of the spline-based motion model on the *dog* video of DAVIS2016 dataset (with  $K = 4$ ). From top to bottom: input flows of the sequence; corresponding predicted motion segmentation maps; flows reconstructed with the space-time polynomial motion model; plots over time of the mean-value of the  $u$ -components of the flows provided per segment by the space-time polynomial motion models; plots over time of the mean-value of the  $v$ -components of the flows provided per segment by the space-time polynomial motion models; flows reconstructed with the space-time spline-based motion model; plots over time of the mean-value of the  $u$ -components of the flows provided per segment by the spline-based motion models; plots over time of the mean-value of the  $v$ -components of the flows provided per segment by the spline-based motion models. Clearly, the space-time polynomial model fails to handle non-uniformly varying motion, whereas the spline-based model does.

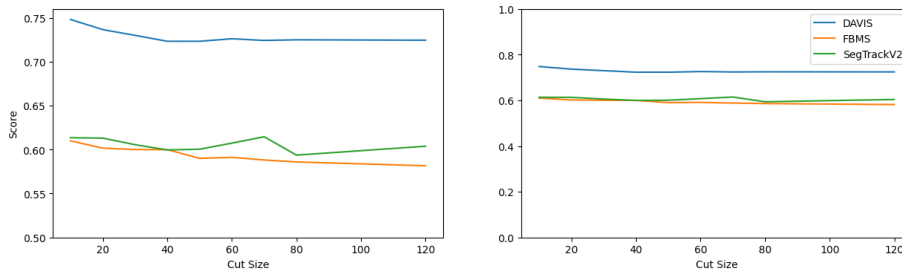


Figure 8: Influence of the length of the input flow sequence (also referred to as cut size on the horizontal axis of the plot) on the LT-MS-K4 method for three datasets, DAVIS2016, FBMS59 and SegTrackV2. As expected, the best performance is obtained for the smallest length (cut size equal to 10), but performance decreases slowly when the cut size increases and remains stable for larger ones. On the right, the plot is shown with the full range of values on the ordinate  $[0, 100]$ . On the left, a zoomed-in version of the plot.

## 7.8 Repeatability

With the introduction of the transformer decoder, we experimentally found that the convergence of the network depends on the weights initialization, and that the same network and loss configuration can yield different results at test time. In Fig.11, we show that our unsupervised loss on a held-out validation set is a good indicator of the network performance at test time. This is a critical point for model and hyperparameter selection, since we do not have access to the ground truth at training time (with our fully unsupervised scenario), and thus we cannot evaluate model performance. Fig.12 plots the model performance after training as a function of the initialization budget.

In our evaluation experiments, we account for this randomness by training five models with the same set of seeds for all ablations and by reporting the score of the model with the lowest validation loss for each model.

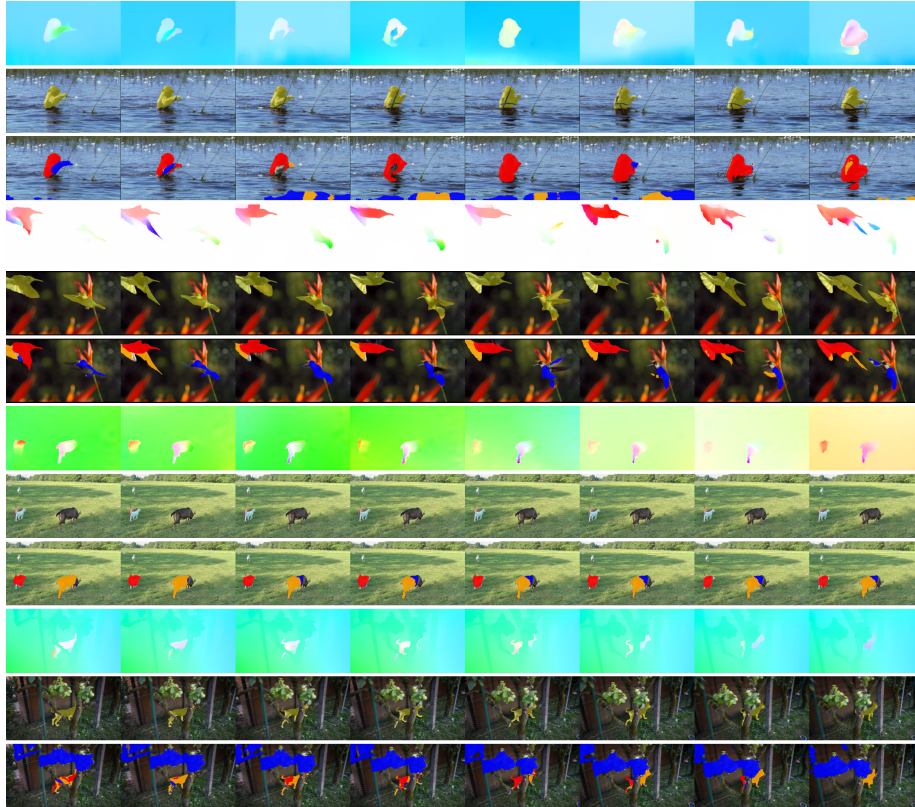


Figure 9: Results obtained with our LT-MS-K4 method ( $K = 4$ ). Four groups of results are displayed: *monkey*, *hummingbird* from SegTrackV2, *goats01* from FBMS59 and *libby* from DAVIS2016. For each group, the first row samples successive flow fields (HSV color code) corresponding to the processed video. The second row contains the corresponding images of the video, where the ground-truth of the moving object is overlaid in yellow (when available at that frame). The third row shows the motion segments provided by our LT-MS-K4 method with one colour per segment. For all the results, we adopt the same color set for the three masks corresponding to the moving objects (blue, red and orange), and we let the background image for the background mask.



Figure 10: Illustration of the temporal consistency provided by our LT-MS-K4 method for three examples, the *birdfall*, *bird-of-paradise*, and *bmx* videos of SegTrackV2. For each group, the first row contains the video images with the ground truth overlaid in yellow when available; the second row depicts the corresponding flow fields represented with the HSV code while normalized independently from each other; the third row provides the predicted segmentation.

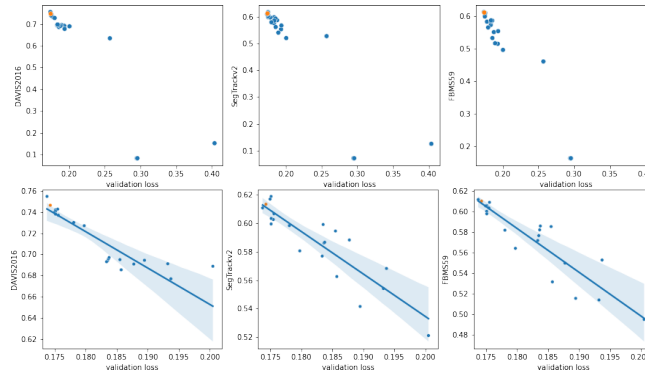


Figure 11: Model scores depending on initialization. Each dot represents a trained model. The  $x$ -axis represents the validation loss on the DAVIS 2016 train dataset, and the  $y$ -axis the performance on the evaluation dataset. The top row includes all models and the bottom row excludes models that diverged during training (validation loss  $> 0.25$ ). The bottom row displays the linear relationship between validation loss and evaluation score. The model whose results are reported in the main text is represented as an orange dot.

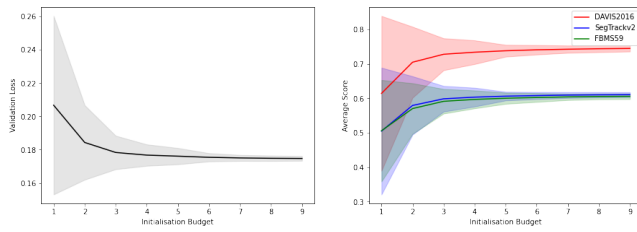


Figure 12: Evolution of the model performance as a function of the initialization budget. Left : the validation loss associated to the best network of each subset. Right : average performance on the test data set associated to this network for each different budget. The filled area correspond to +/- the standard deviation for each curve.

## References

- [1] G.K. Batchelor. *An introduction to fluid dynamics*. Cambridge University Press, 1967.
- [2] D.J. Butler, J. Wulff, G.B. Stanley, and M.J. Black. A naturalistic open source movie for optical flow evaluation, In *European Conference on Computer Vision (ECCV)*, 2012.
- [3] M. Caron, H. Touvron, I. Misra, H. Jégou, J. Mairal, P. Bojanowski, and A. Joulin. Emerging properties in self-supervised vision transformers. In *International Conference on Computer Vision (ICCV)*, October 2021.
- [4] B. Cheng, A. G. Schwing, and A. Kirillov. Per-pixel classification is not all you need for semantic segmentation. In *Conference on Neural Information Processing Systems (NeurIPS)*, 2021.
- [5] J. Cheng, Y.-H. Tsai, S. Wang, and M.-H. Yang. Segflow: Joint learning for video object segmentation and optical flow. In *International Conference on Computer Vision (ICCV)*, Venice, 2017.
- [6] S. Choudhury, L. Karazija, I. Laina, A. Vedaldi, and C. Rupprecht. Guess what moves: Unsupervised video and image segmentation by anticipating motion. *British Machine Vision Conference (BMVC)*, London, 2022.
- [7] A. Dave, P. Tokmakov, and D. Ramanan. Towards segmenting anything that moves. In *Int. Conference on Computer Vision Workshops (ICCVW)*, Seoul, 2019.
- [8] S. Ding, W. Xie, Y. Chen, R. Qian, X. Zhang, H. Xiong, and Q. Tian. Motion-inductive self-supervised object discovery in videos. *arxiv.org/abs/2210.00221*, October 2022.
- [9] B. Duke, A. Ahmed, C. Wolf, P. Aarabi, and G. W. Taylor. SSTVOS: Sparse spatiotemporal transformers for video object segmentation. In *Conference on Computer Vision and Pattern Recognition (CVPR)*, 2021.
- [10] B. Griffin and J. Corso. Tukey-inspired video object segmentation. In *IEEE Winter Conference on Applications of Computer Vision (WACV)*, Waikoloa Village, January 2019.
- [11] K. Han, Y. Wang, H. Chen, X. Chen, J. Guo, Z. Liu, Y. Tang, A. Xiao, C. Xu, Y. Xu, Z. Yang, Y. Zhang, and D. Tao. A survey on vision transformer. *IEEE Transactions on Pattern Analysis and Machine Intelligence*, 45(1):87-110, January 2023.
- [12] S.D. Jain, B. Xiong, and K. Grauman. FusionSeg: Learning to combine motion and appearance for fully automatic segmentation of generic objects in videos. In *Conference on Computer Vision and Pattern Recognition (CVPR)*, Honolulu, 2017.
- [13] D.P. Kingma and M. Welling. An introduction to variational autoencoders. *Foundations and Trends in Machine Learning*, 12(4):307-392, 2019.
- [14] D. Lao, Z. Hu, F. Locatello, Y. Yang, and S. Soatto. Divided attention: Unsupervised multi-object discovery with contextually separated slots. *arXiv:2304.01430*, April 2023.
- [15] F. Li, T. Kim, A. Humayun, D. Tsai, and J. M. Rehg. Video segmentation by tracking many figure-ground segments. In *International Conference on Computer Vision (ICCV)*, Sydney, 2013.
- [16] L. Lian, Z. Wu, S. X. Yu. Bootstrapping objectness from videos by relaxed common fate and visual grouping. *Conference on Computer Vision and Pattern Recognition*, Vancouver, June 2023.
- [17] R. Liu, Z. Wu, S. X. Yu, and S. Lin. The Emergence of objectness: Learning zero-shot segmentation from videos. In *Conference on Neural Information Processing Systems (NeurIPS)*, 2021.

- [18] F. Locatello, D. Weissenborn, T. Unterthiner, A. Mahendran, G. Heigold, J. Uszkoreit, A. Dosovitskiy, and T. Kipf. Object-centric learning with slot attention. In *Conference on Neural Information Processing Systems (NeurIPS)*, 2020.
- [19] J. Mattheus, H. Grobler, and A. M. Abu-Mahfouz. A review of motion segmentation: Approaches and major challenges. *International Multidisciplinary Information Technology and Engineering Conference (IMITEC)*, November 2020.
- [20] N. Mayer, E. Ilg, P. Häusser, P. Fischer, D. Cremers, A. Dosovitskiy and T. Brox. A large dataset to train convolutional networks for disparity, optical flow, and scene flow estimation. In *Conference on Computer Vision and Pattern Recognition (CVPR)*, Las Vegas, June 2016.
- [21] E. Meunier, A. Badoual and P. Bouthemy. EM-driven unsupervised learning for efficient motion segmentation. In *IEEE Transactions on Pattern Analysis and Machine Intelligence*, 45(4):4462-4473, April 2023.
- [22] E. Meunier and P. Bouthemy. Unsupervised space-time network for temporally-consistent segmentation of multiple motions. In *Conference on Computer Vision and Pattern Recognition (CVPR)*, Vancouver, June 2023.
- [23] A. Mitiche and P. Bouthemy. Computation and analysis of image motion: A synopsis of current problems and methods. *International Journal of Computer Vision*, 19(1):29-55, 1996.
- [24] P. Ochs, J. Malik, and T. Brox. Segmentation of moving objects by long term video analysis. *IEEE Transactions on Pattern Analysis and Machine Intelligence*, 36(6):1187-1200, June 2014.
- [25] A. Papazoglou and V. Ferrari. Fast object segmentation in unconstrained video. In *IEEE International Conference on Computer Vision (ICCV)*, Sydney, December 2013.
- [26] F. Perazzi, J. Pont-Tuset, B. Mc Williams, L. Van Gool, M. Gross, and A. Sorkine-Hornung. A benchmark dataset and evaluation methodology for video object segmentation. In *Conf. on Computer Vision and Pattern Recognition (CVPR)*, Las Vegas, June 2016.
- [27] J. Pont-Tuset, F. Perazzi, S. Caelles, P. Arbeláez, A. Sorkine-Hornung, and L. Van Gool. The 2017 Davis challenge on video object segmentation. *arXiv:1704.00675*, 2017.
- [28] A. Ranjan, V. Jampani, L. Balles, K. Kim, D. Sun, J. Wulff, and M.J. Black. Competitive collaboration: Joint unsupervised learning of depth, camera motion, optical flow and motion segmentation. In *Conf. on Computer Vision and Pattern Recognition (CVPR)*, Long Beach, 2019.
- [29] O. Ronneberger, P. Fischer, and T. Brox. U-net: Convolutional networks for biomedical image segmentation. In *Int. Conf. on Medical Image Computing and Computer Assisted Intervention (MICCAI)*, Munich, October 2015.
- [30] D. Sun, E. B. Sudderth, and M. J. Black. Layered segmentation and optical flow estimation over time. In *Conference on Computer Vision and Pattern Recognition (CVPR)*, Providence, June 2012.
- [31] Z. Teed and J. Deng. RAFT: Recurrent all-pairs field transforms for optical flow. In *European Conference on Computer Vision (ECCV)*, 2020.
- [32] M. Unser. Splines: A perfect fit for signal and image processing. *Signal Processing Magazine*, 16(6):22-38, November 1999.
- [33] J. Xie, W. Xie, and A. Zisserman. Segmenting moving objects via an object-centric layered representation. In *Conference on Neural Information Processing Systems (NeurIPS)*, 2022.

- [34] X. Xu, L. Zhang, L.-F. Cheong, Z. Li, and C. Zhu. Learning clustering for motion segmentation. *IEEE Transactions on Circuits and Systems for Video Technology*, 32(3):908-919, March 2022.
- [35] C. Yang, H. Lamdouar, E. Lu, A. Zisserman, and W. Xie. Self-supervised video object segmentation by motion grouping. In *International Conference on Computer Vision (ICCV)*, October 2021.
- [36] Y. Yang, A. Loquercio, D. Scaramuzza, and S. Soatto. Unsupervised moving object detection via contextual information separation. In *Conference on Computer Vision and Pattern Recognition (CVPR)*, Long Beach, 2019.
- [37] Y. Yang, B. Lai, and S. Soatto. DyStAB: Unsupervised object segmentation via dynamic-static bootstrapping. In *Conference on Computer Vision and Pattern Recognition (CVPR)*, 2021.
- [38] L. Zappella, X. Llado, and J. Salvi. Motion segmentation: A review. *Frontiers in Artificial Intelligence and Applications*, 184:(398-407), January 2008.
- [39] T. Zhou, F. Porikli, D.J. Crandall, L. Van Gool, and W. Wang. A survey on deep learning technique for video segmentation. *IEEE Transactions on Pattern Analysis and Machine Intelligence*, 45(6):7099-7122, June 2023.
- [40] D. Liu and J. Nocedal. On the limited memory BFGS method for large scale optimization. In *Mathematical Programming*, 45(1-3):503-528, 1989.